AIChE

Detached Eddy Simulation on the Turbulent Flow in a Stirred Tank

J. Gimbun
Faculty of Chemical and Natural Resources Engineering, Universiti Malaysia Pahang, Lebuhraya Tun Razak, 26300 Gambang, Pahang, Malaysia

Dept. Chemical Engineering, Loughborough University, Leics, LE11 3TU, U.K.

C. D. Rielly and Z. K. Nagy
Dept. Chemical Engineering, Loughborough University, Leics, LE11 3TU, U.K.

J. J. Derksen
Dept. Chemical and Materials Engineering, University of Alberta, Edmonton, AB, Canada T6G 2G6

DOI 10.1002/aic.12807
Published online November 28, 2011 in Wiley Online Library (wileyonlinelibrary.com).

A detached eddy simulation (DES), a large-eddy simulation (LES), and a k-ε*-based Reynolds averaged Navier-Stokes (RANS) calculation on the single phase turbulent flow in a fully baffled stirred tank, agitated by a Rushton turbine is presented. The DES used here is based on the Spalart-Allmaras turbulence model solved on a grid containing about a million control volumes. The standard* k-ε *and LES were considered here for comparison purposes. Predictions of the impeller-angle-resolved and time-averaged turbulent flow have been evaluated and compared with data from laser doppler anemometry measurements. The effects of the turbulence model on the predictions of the mean velocity components and the turbulent kinetic energy are most pronounced in the (highly anisotropic) trailing vortex core region, with specifically DES performing well. The LES—that was performed on the same grid as the DES—appears to lack resolution in the boundary layers on the surface of the impeller. The findings suggest that DES provides a more accurate prediction of the features of the turbulent flows in a stirred tank compared with RANS-based models and at the same time alleviates resolution requirements of LES close to walls.* © 2011 American Institute of Chemical Engineers *AIChE J,* 58: 3224–3241, 2012
Keywords: DES, RANS, angle resolved, vortex core, power number, turbulent kinetic energy

Introduction

Stirred tanks are widely used in the chemical and biochemical process industries. Mixing, fermentation, polymerization, crystallization, and liquid–liquid extractions are significant examples of industrial operations usually carried out in tanks agitated by one or more impellers. The flow phenomena inside the tank are of great importance in the design, scale-up, and optimization of tasks performed by stirred tanks.

Although several advanced experimental methods such as laser doppler anemometry (LDA) and particle image velocimetry (PIV) are capable of evaluating the turbulent flow phenomena in stirred tanks, these methods have their specific limitations. PIV and LDA techniques cannot be applied to opaque fluids, under hazardous conditions, in nontransparent vessels or when the system is sensitive to laser radiation. Computational fluid dynamics (CFD) presents an alternative quantitative route of describing stirred-tank flow, although modeling of dense multiphase flows and fluids with complex rheology is still troublesome. In addition, geometrical complexity and the, in many cases, turbulent nature of the flow makes that CFD results need to be critically assessed, e.g., by comparing them with experimental data. Once sufficiently validated, CFD provides a powerful tool for investigating flows and supporting process design at a lower expense than would be required by a high-quality experimental facility.

Before dealing with multiphase flows, simulation of the single phase flow in stirred tanks is necessary because the prediction of turbulent flows requires making intricate modeling choices, specifically in complex domains with moving boundaries such as the revolving impeller in a stirred tank. At the same time, good prediction of turbulence quantities (turbulent kinetic energy and turbulent dissipation rate) is important because they strongly influence small-scale processes (chemical reactions and disperse phase behavior such as bubble coalescence and break-up).

Modeling of turbulence in stirred tanks is challenging because the flow structures are highly three-dimensional (3-D) and cover a wide range of spatial and temporal scales. The revolving impeller circulates the fluid through the tank, and there are 3-D vortices formed in the wakes behind the impeller blade.[1] Baffles at the tank wall prevent the liquid from performing a solid-body rotation, thus enhancing the

Correspondence concerning this article should be addressed to J. Gimbun at jolius@ump.edu.my.

mixing, as well as generating strong axial and radial velocity components.

Many researchers[2–10] have studied Reynolds averaged Navier-Stokes (RANS)-based turbulence models (mainly k-ε models) applied to stirred-tank flow. As a general conclusion, these authors claim that CFD satisfactorily predicts mean flow patterns as far as they are associated to axial and radial velocity components, but either under- or over-predicts the flow in the circumferential direction and turbulence quantities, such as the turbulent kinetic energy (k) and the turbulent energy dissipation rate (ε). More elaborate RANS models such as the Reynolds stress model suffer from similar drawbacks.[3,7]

Predictions of tangential velocities have been a problem in simulations of stirred tanks for some time. The tangential velocity fields averaged over all angular impeller positions are usually fairly well represented by CFD. The issues are with the impeller-angle resolved fields and the associated vortex structures in the wakes of impeller blades.

It is possible to fully resolve for the turbulent flow in a stirred tank by direct numerical simulation (DNS). Recently, DNS has been applied to predict the turbulent flow in a stirred tank by Verzicco et al.[11] and Sbrizzai et al.[12] These authors concluded that DNS predicts the turbulence related quantities such as turbulent kinetic energy and turbulent energy dissipation rate much better than RANS models. However, both works involved a low Reynolds number ($Re = 1636$; a transitional flow) in an unbaffled tank, suggesting that DNS for a baffled stirred tank at high Reynolds number is still far beyond the reach of current computer resources.

The main limitation of RANS modeling of turbulently stirred tanks agitated by Rushton turbines is the poor prediction of the turbulence related quantities such as k and ε, and the impeller-angle resolved mean tangential velocity. It is well-known from the literature that large-eddy simulation (LES) is able to better predict the time-averaged flow quantities, including those related to turbulence.[13–23] In a LES, a low-pass filtered version of the Navier-Stokes equation is solved. The fluid motion at the subfilter scales is taken care of by a model. It is a 3-D, transient numerical simulation of turbulent flow, in which the large flow structures are resolved explicitly and the effects of subgrid (or subfilter) scales are modeled, the rationale being that the latter are more universal and isotropic in nature. LESs of stirred-tank flow are computationally expensive. The computational cost of an LES is largely dictated by spatial resolution requirements. Away from walls, the spatial resolution needs to be such that the cut-off spatial frequency of the low-pass filter falls within the inertial subrange of turbulence. In addition, wall-boundary layers need to be sufficiently resolved. It is well-understood that the local Taylor-microscale is a good guide to prepare a grid for LES.[24]

Issues with LES related to boundary layers led to the idea of formulating a turbulence model that is cheaper to run and better predicts turbulent flows, called detached eddy simulation (DES) or hybrid (RANS-LES) turbulence model. The main idea of this approach is to perform LES away from walls where demands on resolution are not that strong, and revert to RANS modeling where LES is not affordable, i.e., in boundary layers. In strong turbulence, flow structures close to the wall are very small[25] and anisotropic. Thus, an LES would need a very fine grid within the boundary layer, which implies that the computational cost does not differ appreciably from that of a DNS anymore.[26] On the other side, inadequate grid resolution of boundary layers can severely degrade the quality of a large eddy simulation. Therefore DES was proposed by Spalart et al.[26] in an attempt to reduce the computational cost as well as to provide a good prediction of turbulent flows, containing boundary layers. A DES is an LES that transfers to a RANS-based simulation in boundary layers, thus permitting a relatively coarse grid near walls. A DES grid differs from a RANS grid and for that purpose Spalart[27,28] has prepared a detailed guide to mesh preparation.

To the authors' knowledge, DES has not yet been used for prediction of single-phase, stirred-tank flows in baffled vessels. The main objective of this work is to assess the quality of DES predictions for stirred-tank flow. For this, a detailed comparison with experimental data in the vicinity of the impeller was performed because in this region the flow is being generated, and here the effect of (in)adequate wall-layer resolution would be most visible. Close to the impeller, boundary layers detaching from impeller blades and associated vortex structures dominate the flow. Impeller-angle resolved data are necessary because their level of detail is required to critically assess performance of DES. In addition to comparing the DES results with experimental data, we also compare them with LES and k-ε results to judge the performance of DES in relation to the latter two (more established and tested) approaches.

Only a few modeling studies that assess the quality of impeller-angle-resolved data with experiments are available in the literature. Li et al.[9] have presented an angle-resolved CFD and LDA comparison on turbulent flows produced by a retreat curve impeller in a tank fitted with a single cylindrical baffle. These authors used a shear-stress-transport (SST) model in their work, which is a combination of the k-ω model near the wall and the k-ε model away from the wall. Tangential velocities and the turbulent kinetic energy were largely under-predicted in their study. Yeoh et al.[16] also have presented an angle-resolved comparison of turbulent flows in a stirred tank. They used a deforming mesh method with LES and reported a good prediction of total kinetic energy. However, there was no comparison made on the angle-resolved random kinetic energy. Hartmann et al.[17] have presented an angle-resolved comparison of turbulent flows generated by a Rushton turbine at a Reynolds number of 7300. The authors compared LES and SST models in their work and concluded that LES predicts both angle-resolved and time-averaged turbulent flow very well. The previous works of Yeoh et al.[16] and Hartmann et al.[17] only presented a limited number of angle-resolved comparisons of turbulent kinetic energy, i.e., for three different angles at a single radial position only. Therefore, such a comparison may not sufficiently take into account the details of the flow around the impeller blades, including trailing vortices.

An accurate prediction of both mean velocities and turbulent quantities in the trailing vortex core is important, as this region plays an important role in the mixing and phase dispersion. It is, therefore, interesting to investigate the capability of various modeling approaches to predict the mean velocities and turbulence-related quantities in the trailing vortex core.

Various aspects of stirred-tanks modeling are discussed in this article, including the ability of turbulence models to predict the angle-averaged and angle-resolved mean flows, turbulence characteristics, trailing vortices, and the power number. The performance of the various models in predicting the

turbulent flow in a single phase stirred tank are identified, with specific attention for the potential of detached-eddy simulations.

The organization of this article is as follows: we start with introducing the flow geometry, the computational grid, and then give a condensed description of the three turbulence modeling approaches (viz. k-ε, LES, and DES) used in this study. In the subsequent "Results and Discussion" section, first, time-averaged velocity data are discussed. Then, we zoom in on the structure of the trailing vortex system associated with the revolving impeller, and we compare the way this vortex system is resolved by the various modeling strategies. The description of the vortex system allows us to interpret the extensive set of impeller-angle-resolved velocity profiles presented next. In the final section of the article, we summarize and reiterate the main conclusions.

Modeling Approach

Tank geometry

The results presented in this work are related to a standard stirred tank configuration, with the tank and impeller dimensions given by Derksen et al.[29] The system is a flat bottomed cylindrical tank, $T = H = 0.288$ m, with four equally spaced baffles. A Rushton turbine with diameter, $D = T/3$, without a hub, was positioned at a bottom clearance of $C = T/3$. The impeller blade and disk thickness was $t = 2$ mm. The impeller was set to rotate with an angular velocity of $N = 3.14$ rps corresponding to a Reynolds number of $Re \equiv \frac{ND^2}{\nu} = 29{,}000$ (with $\nu = 1.0 \times 10^{-6}$ m^2/s the kinematic viscosity of the working fluid which was water). In our coordinate system, the level of $z = 0$ was set to correspond to the impeller disk plane.

Computational grid

GAMBIT 2.2[30] was used to create an unstructured, nonuniform multiblock grid with the impeller (rotating) and static zones being separated by an interface to enable the use of the multiple reference frame (MRF) or sliding grid techniques. The computational grid for the RANS modeling was defined by 516,000 (516k) of structured, nonuniformly distributed hexahedral cells representing (with view to symmetry) only a half-tank domain. A local grid refinement containing 212k cells was applied in the rotating zones to better resolve this highly turbulent region.

The grid for a DES cannot make use of the half-tank and periodic boundary conditions, because here the simulation is fully unsteady and not symmetric. Thus, the existing grid was extended to a full tank grid for the DES. As a result, the extended grid of the whole tank domain contained about a million control volumes (1010k). The DES grid was prepared according to Spalart[27,28] with $y^+ \equiv u_T y/\nu$ ranged from 1 to 33 around the walls defining the impeller. The u_T, y, and ν are the friction velocity, distance from the nearest wall, and the kinematic viscosity, respectively. A grid adaptation is applied around the impeller at $0 < 2r/D < 1.7$ to control the mesh size in this highly turbulent region at $\max(\Delta x, \Delta y, \Delta z) < 0.7$ mm ($= 7.3 \times 10^{-3} D$).

The grid cell size in the impeller region in the current work is smaller than $0.015D$, which is finer than the locally refined grid ($0.023D$) used by Revstedt et al.,[13] who reported a good prediction of turbulence flow using LES. In addition, the Taylor-microscale is well-resolved in the impeller discharged region where 80% of the turbulent kinetics energy dissipates.[14] However, the grid close to impeller wall is not resolved because the main focus of this work is to evaluate the strength of DES for predicting turbulence flow using coarser grid than that for LES. According to Derksen et al.,[29] a proper grid for stirred tanks modeling should be able to resolve the trailing vortex behind the impeller blade. They recommended using at least 8 nodes along the impeller height (corresponding to $0.025D$) to resolve the trailing vortex for RANS modeling. The trailing vortex is an important flow feature in stirred tanks, which significantly affects prediction of the turbulence and mean flow. In this work, 12 nodes along the impeller blade height were assigned for the RANS modeling and 23 nodes were used for the LES and DES modeling. The grid prepared in this work is capable of resolving accurately the radial and axial trailing vortex, as shown in "Identification of the vortex core" section, thus further confirming its suitability.

Turbulence modeling and discretization

The selection of a turbulence model for stirred-tank simulation is very important, especially when dealing with baffled tanks at high Reynolds numbers (strong turbulence). LES is of course an excellent model, but it is still computationally expensive to run on a personal computer, for instance, Delafosse et al.[22] needs 80 days to run LES on a AMD Opteron workstation. Whereas comparatively new turbulence models such as DES need to be validated before they can be applied routinely to stirred-tank modeling. Therefore, the predictive capabilities the most commonly used RANS model, i.e., the standard k-ε as well as DES and LES, on turbulent flows in a single-phase stirred tank have been extensively compared in this study. These models are described in more detail below.

The standard k-ε model is based on transport equations for the turbulent kinetic energy and its dissipation rate. Transport equations for k and ε for all k-ε variant models can be generalized as follow:

$$\underbrace{\frac{\partial(\rho k)}{\partial t}}_{\text{time derivative}} + \underbrace{\frac{\partial}{\partial x_i}(\rho u_i k)}_{\text{convection}} = \underbrace{\frac{\partial}{\partial x_i}\left(\left(\mu + \frac{\mu_t}{\sigma_k}\right)\frac{\partial k}{\partial x_i}\right)}_{\text{diffusion}} + \underbrace{\rho P_k}_{\text{production}} - \underbrace{\rho\varepsilon}_{\text{destruction}} \tag{1}$$

and

$$\underbrace{\frac{\partial(\rho\varepsilon)}{\partial t}}_{\text{time derivative}} + \underbrace{\frac{\partial}{\partial x_i}(\rho u_i \varepsilon)}_{\text{convection}} = \underbrace{\frac{\partial}{\partial x_i}\left(\left(\mu + \frac{\mu_t}{\sigma_\varepsilon}\right)\frac{\partial \varepsilon}{\partial x_i}\right)}_{\text{diffusion}} + \underbrace{S_\varepsilon}_{\text{source term}} \tag{2}$$

The turbulent (eddy) viscosity, μ_t, is obtained from:

$$\mu_t = \rho C_\mu \frac{k^2}{\varepsilon} \tag{3}$$

The relation for the production term, P_k, for the k-ε model is given as:

$$P_k = \mu_t\left(\frac{\partial u_j}{\partial x_i} + \frac{\partial u_i}{\partial x_j}\right)\frac{\partial u_j}{\partial x_i} \tag{4}$$

For the standard k-ε model, the source term, S_e, is given by:

$$S_\varepsilon = \rho\left(C_{1\varepsilon}\frac{\varepsilon}{k}P_k - C_{2\varepsilon}\frac{\varepsilon^2}{k}\right) \tag{5}$$

The model constants are[31]: $C_{\varepsilon 1} = 1.44$, $C_{\varepsilon 2} = 1.92$, $C_\mu = 0.99$, $\sigma_k = 1$, and $\sigma_\varepsilon = 1.3$ derived from correlations of experimental data.

In LES, it is assumed that the large eddies of the flow are dependent on the flow geometry and boundary conditions, whereas the smaller eddies are self-similar and have a universal character. Thus, in LES, the large unsteady vortices are solved directly by the filtered Navier-Stokes equations, whereas the effect of the smaller universal scales [subgrid scales (SGSs)] are modeled using a SGS model. The filtered Navier-Stokes equation is given by:

$$\frac{\partial \bar{u}_i}{\partial t} + \frac{\partial}{\partial x_j}\left(\bar{u}_i\,\bar{u}_j\right) = \frac{1}{Re}\frac{\partial^2 \bar{u}_i}{\partial x_j^2} - \frac{\partial \tau_{ij}^{\mathrm{SGS}}}{\partial x_j} - \frac{\partial \bar{p}}{\partial x_i} \tag{6}$$

where τ_{ij}^{SGS} is the SGS stress modeled by:

$$\tau_{ij}^{\mathrm{SGS}} - \frac{1}{3}\tau_{kk}^{\mathrm{SGS}}\,\delta_{ij} = -2\mu_{\mathrm{t}}^{\mathrm{SGS}}\bar{S}_{ij} \tag{7}$$

The $\mu_{\mathrm{t}}^{\mathrm{SGS}}$ is the SGS turbulent viscosity, and $\bar{S}_{ij}$, is rate-of-strain tensor for the resolved velocity field defined as:

$$\bar{S}_{ij} = \frac{1}{2}\left(\frac{\partial \bar{u}_i}{\partial x_j} + \frac{\partial \bar{u}_j}{\partial x_i}\right) \tag{8}$$

The overbars in Eqs. 6–9 denote resolved scale quantities rather than time-averages. The most commonly used SGS model is the Smagorinsky[32] model, which has been further developed by Lilly.[33] It compensates for the unresolved turbulent scales through the addition of an isotropic turbulent viscosity into the governing equations. In the Smagorinsky-Lilly model, the turbulent viscosity is modeled by:

$$\mu_{\mathrm{t}}^{\mathrm{SGS}} = \rho L_{\mathrm{s}}^2\,|\bar{S}| \tag{9}$$

where L_{s} is the mixing length for SGSs and $|\bar{S}| = \sqrt{2\bar{S}_{ij}\bar{S}_{ij}}$. L_{s} can be calculated from:

$$L_{\mathrm{s}} = \min\left(\kappa d, C_{\mathrm{s}}V^{1/3}\right) \tag{10}$$

where $\kappa = 0.42$, d is the distance to the nearest wall, C_{s} is the Smagorinsky constant, and V is the volume of the computational cell. The Smagorinsky constant was set to 0.1, which is a commonly applied value for shear-driven turbulence. The Smagorinsky constant was set at 0.2 in the newer version of Fluent Ansys R13, which could have been motivated by findings by Delafosse et al.[22] who shows a better prediction of turbulent dissipation rate from LES can be obtained by adjusting the constant C_{s} in the Smagorinsky model from 0.1 to 0.2. A LES was performed in this work to evaluate the effect of unresolved eddies near the impeller wall on the turbulence and mean velocities predictions. It has to be noted that the y^+ around the impeller wall in this work ranged from 5 to 40, which is not well-resolved for LES. To the best of our knowledge, the effect of the unresolved eddies near the impeller wall on the LES prediction has not been evaluated comprehensively for a stirred-tank flow, especially not in terms of angle-resolved flow quantities.

DES, as mentioned earlier, belongs to a class of a hybrid turbulence model, which blend LES in flow regions away from boundary layers with RANS near the wall. This approach was introduced by Spalart et al.[26] in an effort to reduce the overall computational effort of LES modeling by allowing a coarser grid within the boundary layers. The DES used in this work is based on the Spalart-Allmaras (SA) model.[34]

The SA one-equation model solves a single partial differential equation (Eq. 11) for a variable $\tilde{\nu}$, which is called the modified turbulent viscosity. The variable $\tilde{\nu}$ is related to the eddy viscosity by Eq. 12 with additional viscous damping function f_{v1} to ensure the eddy viscosity is predicted well in both the log layer and the viscous-affected region. The model includes a destruction term that reduces the turbulent viscosity in the log layer and laminar sublayer. The transport equation for $\tilde{\nu}$ in DES is:

$$\begin{aligned}&\frac{\partial}{\partial t}(\rho\tilde{\nu}) + \frac{\partial}{\partial x_i}(\rho\tilde{\nu}u_i)\\ &= G_\nu + \frac{1}{\sigma_{\tilde{\nu}}}\left[\frac{\partial}{\partial x_j}\left\{(\mu+\rho\tilde{\nu})\frac{\partial\tilde{\nu}}{\partial x_j}\right\} + C_{b2}\rho\left(\frac{\partial\tilde{\nu}}{\partial x_j}\right)^2\right] - Y_\nu\end{aligned} \tag{11}$$

The turbulent viscosity is determined via:

$$\mu_{\mathrm{t}} = \rho\tilde{\nu}f_{v1}, \quad f_{v1} = \frac{\chi^3}{\chi^3 + C_{v1}^3}, \quad \chi \equiv \frac{\tilde{\nu}}{\nu} \tag{12}$$

where $\nu = \mu/\rho$ is the molecular kinematic viscosity. The production term, G_ν, is modeled as:

$$G_\nu = C_{b1}\rho\tilde{S}\tilde{\nu}, \quad \tilde{S} \equiv S + \frac{\tilde{\nu}}{k^2d^2}f_{v2}, \quad f_{v2} = 1 - \frac{\chi}{1+\chi f_{v1}} \tag{13}$$

S is a scalar measure of the deformation rate tensor, which is based on the vorticity magnitude in the SA model. The destruction term is modeled as:

$$\begin{aligned}&Y_\nu = C_{w1}\rho f_w\left(\frac{\tilde{\nu}}{d}\right)^2, \quad f_w = g\left[\frac{1+C_{w3}^6}{g^6+C_{w3}^6}\right]^{1/6},\\ &g = r + C_{w2}\left(r^6 - r\right), \quad r \equiv \frac{\tilde{\nu}}{\tilde{S}k^2d^2}\end{aligned} \tag{14}$$

The closure coefficients for SA model[34] are $C_{b1} = 0.1355$, $C_{b2} = 0.622$, $\sigma_{\tilde{\nu}} = \frac{2}{3}$, $C_{v1} = 7.1$, $C_{w1} = \frac{C_{b1}}{k^2} + \frac{(1+C_{b2})}{\sigma_{\tilde{\nu}}}$, $C_{w2} = 0.3$, $C_{w3} = 2.0$, $k = 0.4187$.

In the SA model, the destruction term (Eq. 14) is proportional to $(\tilde{\nu}/d)^2$. When this term is balanced with the production term, the eddy viscosity becomes proportional to $\tilde{S}d^2$. The Smagorinsky LES model varies its SGS turbulent viscosity with the local strain rate, and the grid spacing is described by $\nu_{\mathrm{SGS}} \propto \tilde{S}\Delta^2$ in Eq. 9, where $\Delta = \max(\Delta x, \Delta y, \Delta z)$. If d is replaced with Δ in the wall destruction term, the SA model will act like a LES model. To exhibit both RANS and LES behavior, d in the SA model is replaced by:

$$\tilde{d} = \min(d, C_{\text{des}}\Delta) \quad (15)$$

where C_{des} is a constant with a value of 0.65. Then, the distance to the closest wall d in the SA model is replaced with the new length scale $\tilde{d}$ to obtain the DES. The purpose of using this new length is that in boundary layers where Δ by far exceeds d, the standard SA model applies as $\tilde{d} = d$. Away from walls where $\tilde{d} = C_{\text{des}}\Delta$, the model turns into a simple one equation SGS model, close to Smagorinsky's in the sense that both make the mixing length proportional to Δ. The Smagorinsky model is the standard eddy viscosity model for LES. On the other hand, this approach retains the full sensitivity of RANS model predictions in the boundary layer. This model has not yet been applied to predict stirred tank flows. Applying DES and assessing its performance in relation to experimental data and other turbulence modeling approaches is the main objective of this study.

Modeling strategy

A MRF model[35] was applied to represent the impeller rotation for all the RANS simulations, with a second-order discretization scheme and standard wall functions. The bounded central differencing (BCD) scheme was applied for spatial discretization of the momentum equations for the DES modeling, and time-advancement was achieved by a second-order accurate implicit scheme. The central differencing scheme is an ideal choice for LES due to its lower numerical diffusion. However, it often leads to unphysical oscillations in the solution field.[36] The BCD scheme was introduced to reduce these unphysical oscillations. BCD blends the pure central differencing scheme with first- and second-order upwind schemes. The first-order scheme is applied only when the convection boundedness criterion is violated.[36]

The transient impeller motion for the DES study was modeled using the sliding mesh scheme. PRESTO[37] was applied for pressure-velocity coupling for all cases, as it is optimized for swirling and rotating flow.[36] The DES modeling was initialized using the data from a k-ε simulation. A text user interface command was used to generate the instantaneous velocity field out of the steady-state RANS results. This command must be executed before DES is enabled to create a more realistic initial field for the DES run. This step is necessary to reduce the time needed for the DES simulation to reach a statistically steady-state. Apart from the DES modeling, a LES study was also carried out for comparison. The LES and DES were solved using the same grid because the main aim of this work was to carry out the simulation using a fairly coarse grid ($y^+ \sim 20$), where the DES should be working well. The LES was initialized using the final data from the DES simulation.

The time step and the number of iterations are crucial in both DES and LES modeling because they involve a transient solution. The time step must be small enough to capture all flow features induced by the motion of the impeller blades. Selection of the time step would not be clear without a review of some recent LES studies on stirred tanks. The time steps for LES simulations taken from the literature were normalized with the impeller speed (ΔtN) to make the value dimensionless. Ref. 13 used a ΔtN of 0.0027, Ref. 23 used a ΔtN of 0.0083, and Ref. 16 used a ΔtN of 0.0046. FLUENT[36] recommends that in one time step the sliding interface should move by no more than one grid spacing to get a stable solution. In this study, a ΔtN of 0.00278 was used throughout the final simulation corresponding to 1° impeller movement for the LES and DES simulation. The grid size at the sliding interface was set at 0.002 m, and the circumference of the interface was 0.69 m. Thus, one grid cell movement per time step would require a ΔtN of 0.00289, which is larger than the one used in this work. About 7 s of actual time was simulated corresponding to about 22 impeller revolutions. Before that, about 145 impeller revolutions had been simulated using a ΔtN of 0.00833 corresponding to 3° of impeller movement. The instantaneous velocity and torque acting on the impeller surface were monitored throughout the simulation, and the data presented in this work were taken after the statistical convergence has been achieved. About 10 s of actual time has been simulated for a time step corresponding to 1° impeller movement for the LES modeling starting from the final DES flow field. The three instantaneous velocity components were recorded at every time step at various monitoring points (analogous to LDA measurements) and data extraction on a plane (analogous to 3D PIV as all the 3-D velocity component can be obtained). Postprocessing of the DES and LES data were performed using a Visual Basic code embedded in MS Excel.

Results and Discussions

The CFD simulations of a Rushton turbine described in this article were compared with the experimental LDA results reported by Derksen et al.[29] The three component LDA data used for these validation purposes were angle-resolved mean and fluctuating velocities taken at 3° intervals of blade rotation, starting from 1° behind the blade (see Ref. 29 for details). All data of the mean velocity, k and ε were made dimensionless by dividing them by V_{tip}, V_{tip}^2, or N^3D^2, respectively. The LDA data were processed as time-averaged, angle-resolved mean and turbulence quantities.

A grid analysis was not performed in this article but the prepared grid was assumed to be fine enough to yield a grid independent solution. According to Derksen and Van den Akker,[14] about 80% of the turbulence generated by a rotating impeller is dissipated within the impeller swept volume and the impeller discharge region. Derksen et al.[29] also stated that the trailing vortex behind the impeller blade must be well resolved to obtain a reasonable prediction of the turbulence and mean velocities. They suggested at least 8 nodes should be placed along the impeller blade height to resolve the trailing vortex, and the grid used in this work was prepared sufficiently fine with 12 nodes for the RANS simulation and 23 nodes for the DES and LES simulation (see earlier discussions in "Computational grid" section). A grid analysis performed in our previous work[38] based on the grid refinement around the impeller and its discharge region also confirmed the suitability of the prepared grid to produce a grid independent solution.

CFD results for the time-averaged and impeller-angle-resolved single phase turbulent flow are discussed extensively in this section. All results presented are taken from a well converged simulation, where the normalized residuals have fallen below 1×10^{-3} for all RANS model simulations. RANS was chosen in this work instead of unsteady Reynolds averaged Navier-Stokes (URANS) because there is a limited difference from the result obtained using either URANS or RANS.[16,17] Moreover, URANS requires longer iteration because they require a solution from unsteady

sliding mesh. Of course, there is no such convergence criterion for the transient simulations using DES and LES. However, a sufficient number of iterations per time step (up to 35 iterations per time step) have been applied to make sure the residuals fell below 1×10^{-3} at each time step. The results for the DES and LES presented here were averaged over the 4 final impeller revolutions after the statistical convergence on the instantaneous velocity was achieved. Four impeller revolutions are sufficient for postprocessing if the flows are already in pseudo-steady condition (e.g., 2.5 revolutions used by Alcamo et al.[23]).

Angle-resolved result near the impeller tip and in the impeller out stream (from $2r/D = 1.1$–1.52) for mean velocities and turbulent kinetic energy are compared with the angle-resolved LDA experiments. A broad range of angle-resolved comparisons are necessary to capture the effect of the trailing vortex core on the prediction of mean and turbulent flow quantities. With a view to extending our work to multiphase systems, the accuracy of such CFD prediction in multiphase flows might be critically dependent on proper simulation of the trailing vortex core. A detailed comparison between the CFD predictions and the published measurements, very close to the impeller tip is presented in this section. The effects of the vortex core on the prediction of mean and turbulent flows are accounted by comparing the angle-resolved data and the CFD predictions at different radial positions. Besides the mean and turbulent flow, the axial and radial position of the vortex core were also deduced from the CFD results and compared with Ref. 29.

Time-averaged predictions

Generally, predictions of the LES, DES, and k-ε models used in this study for the time-averaged velocity components (axial, radial, and tangential) were in good agreement with Derksen et al.'s[29] LDA measurements with error $\sim$ 10% as shown in Figure 1. This shows that it is generally easy to predict the mean flow in a stirred tank. Although some discrepancies of the CFD predictions were observed for the impeller-angle-resolved comparisons (as will be discussed in "Prediction of the impeller-angle-resolved flow" section), they apparently where averaged out in the time-averaged results: The CFD predictions are generally good for all angles except for some positions around the trailing vortex core and these discrepancies appear to be marginal when averaged over all azimuthal positions.

The velocity fluctuations in a stirred tank may be categorized as periodic (related to the blade passage) and random (turbulence). As a result, the kinetic energy associated to the fluctuations can be divided in a coherent (k_{coh}) and random (k_{ran}) part. The total kinetic energy (k_{tot}) in the velocity fluctuations is therefore:

$$k_{\text{tot}} = k_{\text{coh}} + k_{\text{ran}} = \frac{1}{2}\left(\overline{u_i^2} - \bar{u}_i^2\right) \tag{16}$$

where u_i is the instantaneous velocity in direction i and $\bar{u}_i$ is the time-averaged velocity. The averages are over all velocity samples irrespective of the angular position of the impeller and the summation convention is applied over the repeated suffix i. The random part of the kinetic energy can be determined if angle-resolved data are available:

$$\overline{k_{\text{ran}}} = \frac{1}{2}\left(\overline{\langle u_i^2\rangle_\theta - \langle u_i\rangle_\theta^2}\right) \tag{17}$$

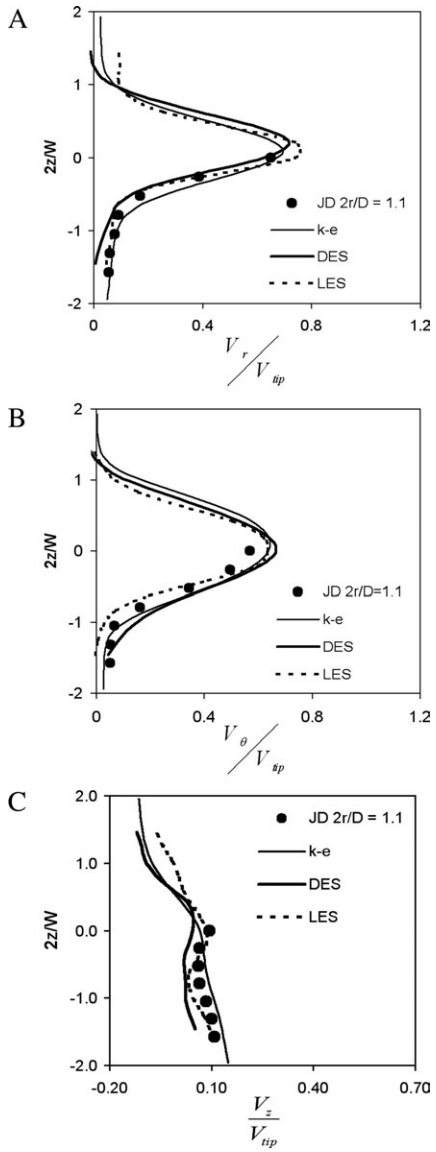

Figure 1. Prediction of time-averaged mean velocity at $2r/D = 1.1$.

Data points are taken from Derksen et al.[29] experimental data.

with $\langle\rangle_\theta$ denotes the average value at impeller angular position θ. The overbar in Eq. 17 denotes averaging over all angular positions (equivalent to time-averaging).

Predictions of the angle-averaged $\overline{k_{\text{ran}}}$ by the k-ε model are about 20% lower than Derksen et al.'s data which is consistent to many other previous works.[7,16,17,22] This is worthwhile highlighting because to the best of our knowledge the k-ε model generally underpredicts $\overline{k_{\text{ran}}}$ by more than 30%. An exception is due to Nere et al.,[39] who empirically adjusted the values of the standard constants in the k-ε model in their study. We do not consider this good practice, because these constants have already been tuned using experimental data and should be retained. The relatively good predictions of $\overline{k_{\text{ran}}}$ by the RANS model in this study are believed to be attributable to the application of a very fine grid around the impeller.

No comparisons can be made for the k_{tot} prediction by the RANS model, because the impeller is actually "frozen" at a

single position in the MRF model. The DES yielded the best prediction of the k_{tot} (see Figure 2) and $\overline{k_{ran}}$ (see Figure 3) with error of less than 5% although prediction by LES away from the impeller ($2r/D = 1.52$) were as good as those obtained from DES. The LES predictions were not very good close to the blade tip ($2r/D = 1.1$) with error up to 20%. This could be due to under-resolved eddies near the impeller wall. The grid was prepared for DES ($y^+ \sim 20$) and (as mentioned earlier) the LES modeling was carried out to compare DES and LES and assess if and to what extend DES improves predictions by better representing boundary layers. At positions closer to the impeller ($2r/D = 1.1$) the DES is capable of producing the double peak in k_{tot} often observed experimentally, whereas the LES fails to show this (although the LES predictions of k_{tot} are still close to the experimental measurements). Similar trends were also observed

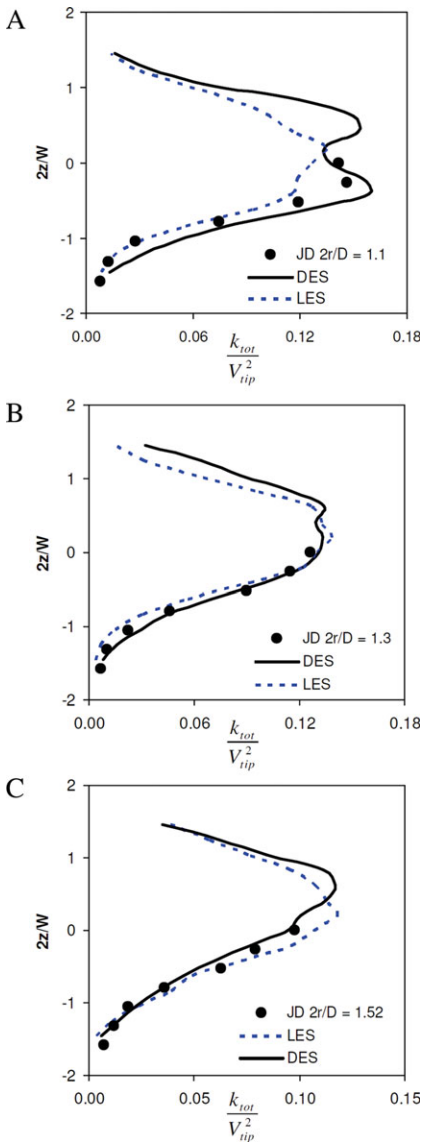

Figure 2. DES and LES prediction of angle-averaged total kinetic energy at three different radial positions.

Data points are taken from Derksen et al.[29] experimental data. [Color figure can be viewed in the online issue, which is available at wileyonlinelibrary.com.]

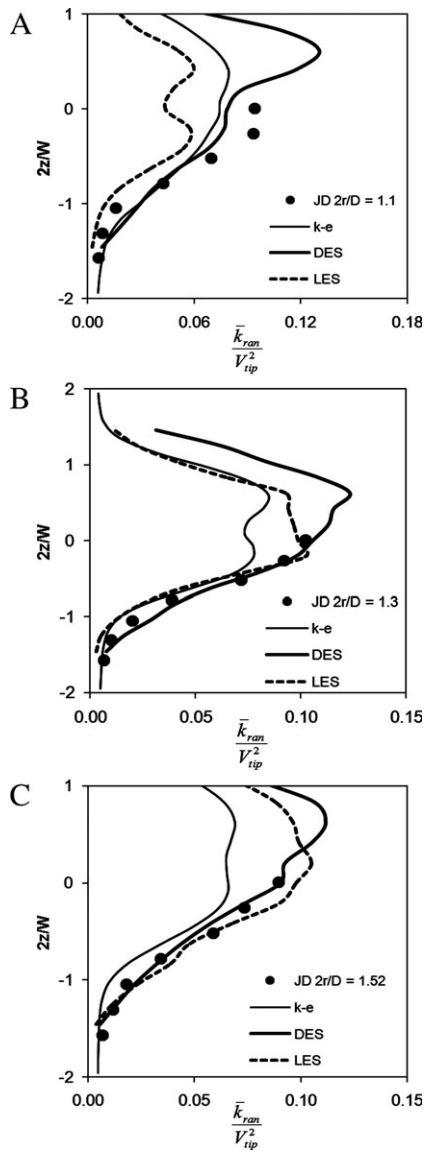

Figure 3. Prediction of $\overline{k_{ran}}$ at three different radial positions, JD corresponds to LDA data from Derksen et al.[29]

for the $\overline{k_{ran}}$ predictions where the LES fails to predict correctly the $\overline{k_{ran}}$ at $2r/D = 1.1$. The k_{tot} is predicted reasonably well by the LES because the k_{tot} is calculated mainly from periodic velocity fluctuation due to the impeller passage, whereas $\overline{k_{ran}}$ depends only on the velocity fluctuations due to the turbulent flow, which explains the poor prediction at $2r/D = 1.1$. The result for $\overline{k_{ran}}$ demonstrates that the grid prepared in this work is not optimal for LES, but it is good for DES. The DES does not need to resolve the small eddies in the boundary layer, because the DES turns into a RANS model in this region and hence works well even for a coarser grid. There are some other studies on LES prediction of turbulent flow in stirred tanks using a relatively coarse grid (e.g., Ref. 16) and they report a good prediction of the turbulent kinetic energy. However, they only presented the k_{tot} which includes the periodic turbulent fluctuation due to the blade passage and they have not presented any comparison for the $\overline{k_{ran}}$ prediction alone. Such an LES study with a coarser grid may not resolve the flow near the boundary

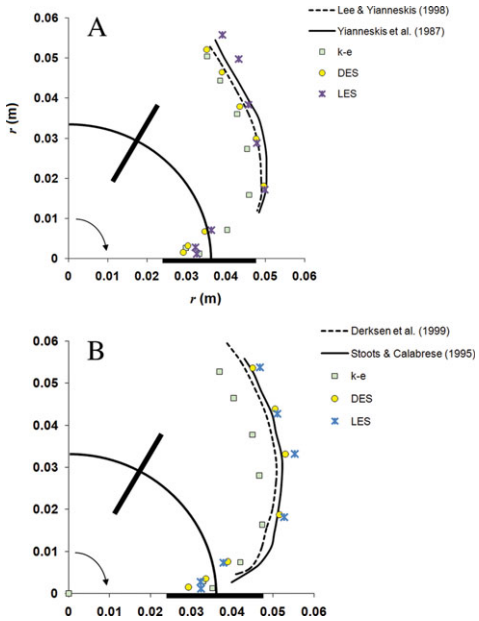

Figure 4. Prediction of the radial trailing vortex core: (A) upper, (B) lower.

[Color figure can be viewed in the online issue, which is available at wileyonlinelibrary.com.]

layer well enough and it may not be able to resolve the $\overline{k_{ran}}$ around the impeller discharge.

Modeling of gas-liquid stirred tank is among the potential application of this study, which requires good predictions of turbulence flow, since they affect prediction of the local bubble size. Correct prediction of the local bubble size is important as they affect directly the hydrodynamics of gas-liquid stirred tank. In this particular application, it is acceptable to have up to 20% error on the turbulence flow prediction because the breakage and coalescence kernel used by the population balance model will not amplify them further. For instance, the commonly used breakage and coalescence kernel for bubble, i.e., Luo,[40] Luo and Svendsen,[41] and Prince and Blanch,[42] has the kinetics of breakage and coalescence depend on ε^a, where $|a|$ is small (0.25 or 0.33). So a 20% error in ε gives rise to less than 5% error in the kinetic rate. In this work, prediction on the mean and turbulence flow is hardly more than 10% for the DES, and therefore, should be acceptable. Moreover, most of the breakage occurs in regions around the impeller, where the turbulence flow is well predicted.

Identification of the vortex core

The vortex core is an important flow feature, which needs to be well represented as it potentially has a great influence on the overall turbulent flow in a stirred tank and (in multiphase applications) the dispersed phase (bubbles, drops, and particles) mixing. For instance, the trailing vortices play a crucial role in determining the gas accumulation behind the impeller,[43] meanwhile, Derksen et al.[29] find that it is impossible to predict accurately the turbulent flow in stirred tanks without resolving accurately the trailing vortices. In turn, this affects the pumping and power dissipation capacity of the impeller and thus significantly affects the performance of a gas-liquid stirred reactor. Furthermore, the trailing vortices were associated with high levels of turbulent activity and high-velocity gradients, and thus play an important role in the mixing capability of a stirred tank.[44]

CFD predictions of the radial position of the trailing vortex core have been published by many researchers.[14,23,45] However, most of the previous studies only consider a single vortex core position (either the upper or lower); the exception is by Derksen and van den Akker[14] who considered both cores. In addition, there has been no extensive CFD comparison made on the axial position of the vortex core with experimental measurements.

A detailed experimental study of the vortex core has been reported previously by Escudie et al.[46] based on the axial and radial positions of the vortex core deduced using three different methods. The first method was called a "null velocity method": the vortex core was obtained simply by connecting the points at which the axial velocity was equal to zero, as proposed by Yianneskis et al.[1] The second method was called the "vorticity method" in which the vortex core position was obtained by connecting the points of maximum vorticity magnitude. The third method, namely, λ_2, was proposed by Jeong and Hussain[47] and was based on the presence of a minimum local pressure in a plane perpendicular to the vortex axis. Escudie et al.[46] found that all three methods gave almost identical curves for the vortex radial position; however, the null velocity method gave a slightly different result compared to both vorticity and λ_2 method for the axial position. The vortex core in this work was determined by using the vorticity method, as it is relatively simple to perform and shows similar results as the λ_2 method.

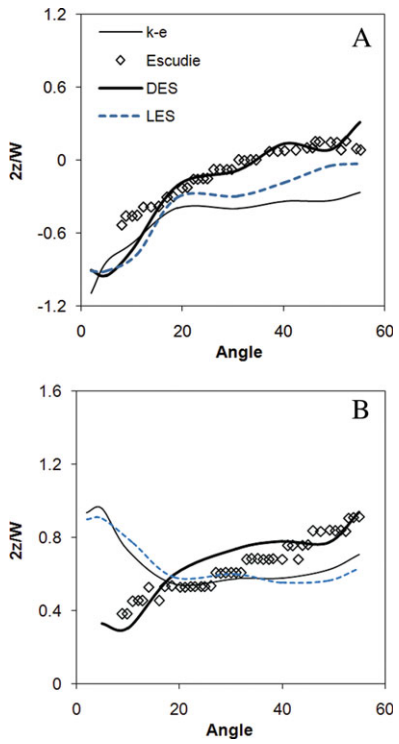

Figure 5. Prediction of the axial movement of the trailing vortex pairs.

Data from Escudie et al.[46] (A) Lower vortex core and (B) upper vortex core. [Color figure can be viewed in the online issue, which is available at wileyonlinelibrary.com.]

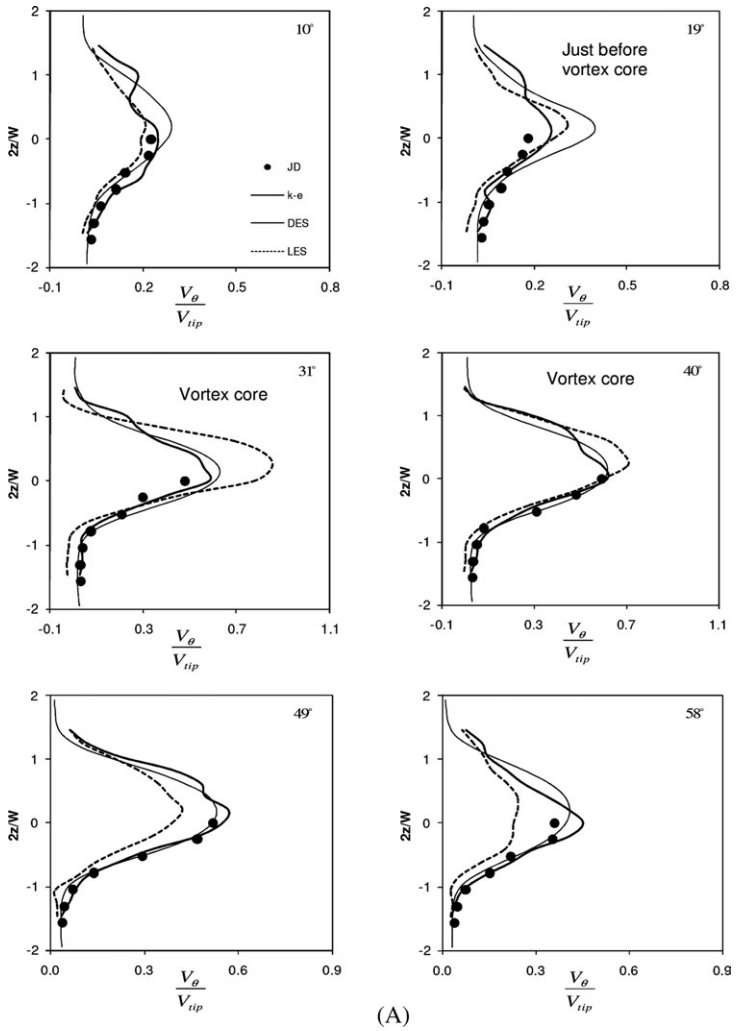

(A)

Figure 6. Prediction of the angle-resolved tangential velocity for different angle positions: (A) at radial position $2r/D = 1.3$, (B) at radial position $2r/D = 1.52$.

JD corresponds to LDA data from Derksen et al.[29]

Data on several planes behind the impeller were exported to independent postprocessing software, SURFER 8, to avoid parallax error from visual assessments of the maximum vorticity position. The vorticity surface plots on a series of *r*-*z* planes at different blade angles were obtained using SURFER 8, and the positions of the vortex core were determined using the build-in digitizer. Postprocessing of the DES data was not as straightforward as for the RANS models, as the instantaneous vorticity magnitudes in the respective *r*-*z* planes (at blade angles 3° to 50°) have to be averaged first before further analysis can be done. A total of 540 instantaneous surface data sets at each blade angle were averaged using Visual Basic code embedded in MS Excel.

Figure 4 shows a comparison of the radial positions of the predicted and the experimental lower and upper vortex cores. The k-ε model provide reasonably good agreement ($\sim$ 7% error) with the results from Derksen et al.[29] for the upper vortex core, but are not as good for the lower vortex core when compared to measurement by Yianneskis et al.[1] with deviation more than 15%. Comparisons are also made with experimental data from other authors, i.e., Refs. 1, 44, 46, and 48. Escudie et al.,[46] Yianneskis et al.,[1] and Lee and Yianneskis[44] worked on a geometrically similar vessel ($D = C = T/3$) to the one evaluated in this article but with slightly different tank diameters: $T = 0.45$ m for Escudie et al.,[46] $T = 0.294$ m for Yianneskis et al.,[1] and $T = 0.1$ m for Lee and Yianneskis.[44] According to Lee and Yianneskis,[44] tanks with geometrically similar dimensions may be able to produce a reasonably similar trailing vortex core, concluding from their results from tanks with diameter of $T = 0.1$ m and $T = 0.294$ m. Meanwhile, Stoots and Calabrese's[48] work was based on a tank with diameter $T = 0.45$ m and $C = T/2$. The CFD predictions in this work were only compared with those obtained using stirred tank with impeller to tank diameter ratio of $D = T/3$ to eliminate an incorrect comparison as the vortex core may also be affected by the D/T ratio. Data from these various authors did show some differences, but they are in close agreement to those from Derksen et al.[29] The DES model gives a good prediction of both the lower and upper vortex core (less than 5% error); slightly better than the k-ε model. It is known that the trailing vortices are amongst the most anisotropic region in a stirred tank, thus demanding the use of a more elaborate turbulence model such as DES or LES. Predictions of LES for the radial position of upper and lower trailing vortices are also in good agreement ($\sim$ 5% error) with experimental data. However, the maximum errors for the LES predictions are slightly

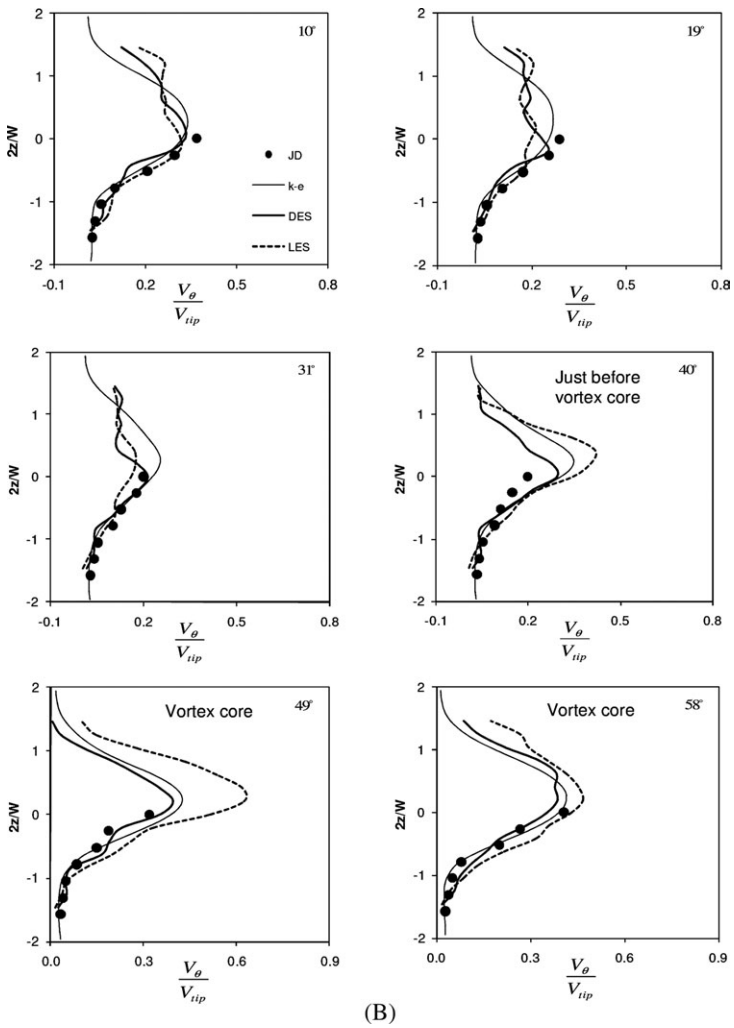

(B)

Figure 6. (Continued)

bigger than those of DES as they are affected by unresolved eddies close to impeller wall.

There are several viewpoints related to the axial position of the vortex core. For example, Yianneskis[1] claimed that the upper vortex core moves at a constant axial position from the top of the impeller at $2z/W = 1$, whereas Derksen et al.[29] claimed that the lower vortex core moves at a constant axial position of $2z/W = -0.52$. Escudie et al.[46] found that both the lower and upper vortex core move axially upward with the lower vortex crossing the impeller centreline ($2z/W = 0$) and moving toward $2z/W = 0.3$; the upper vortex appeared not to move further than $2z/W = 1$. Stoots and Calabrese[48] have studied the axial position of the lower vortex core and they claim that the core was at $2z/W = -0.6$ close to the impeller blade, whereas at larger blade angles, the core moves toward $2z/W \sim -1$. Stoots and Calabrese[48] findings suggest the impeller placement play a big role on the axial position of the lower vortex core as it was found to move downward instead of moving forward when the impeller positioned at $T/2$ instead of $T/3$. It is, therefore, interesting to investigate the capabilities of CFD to predict the axial position of the vortex core in stirred tanks, while bearing in mind the variability of the experimental findings.

Figure 5 shows the predicted axial positions of the vortex core behind the Rushton disk turbine blades. The DES model are in good agreement (less than 10% error) with Escudie et al.'s[46] experiments that involved a similar geometry as the present one (impeller bottom clearance and impeller size is $T/3$). The upward movement of both trailing vortex pairs is successfully predicted by the DES model. The upward vortex movement is as expected, because it is well-known that the discharge flow of the Rushton turbine placed at $T/3$ bottom clearance is inclined slightly upward. It was also noted that the upward movement of the lower vortex core was greater than the upper vortex core. The k-ε model is less successful in predicting the axial position of the vortex core correctly with error up to 30%. Prediction from LES is reasonable for the lower vortex core ($\sim$ 15% error) but is generally poor for the upper vortex core ($\sim$ 30% error). As mentioned earlier this is attributed by unresolved eddies close to impeller wall. The poor predictions of trailing vortex core by LES also explain why LES fails to predict the double peak turbulent kinetics energy close to impeller in Figure 2.

Prediction of the impeller-angle-resolved flow

Before discussion of the angle-resolved comparisons (in Figures 6–9), it is important to relate to the position of the trailing vortices behind the impeller. For reference, two radial positions of $2r/D = 1.3$ and 1.52 are shown. At an angle

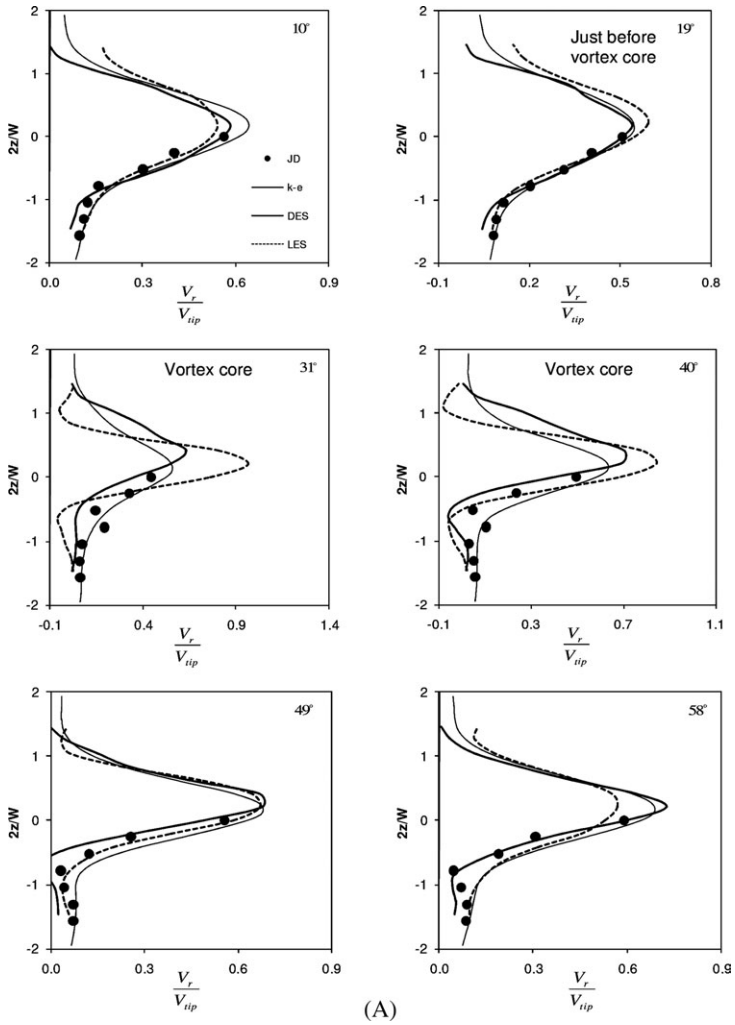

Figure 7. Prediction of the angle-resolved radial velocity for different angle positions: (A) at radial position $2r/D$ = 1.3, (B) at radial position $2r/D$ = 1.52.

JD corresponds to LDA data from Derksen et al.[29]

of around 30° to 50°, vortex cores are near $2r/D = 1.3$ and by around 60° they have reached $2r/D = 1.52$. Predictions of the turbulent kinetics energy especially by the k-ε models are highly affected by the cores of the trailing vortices.

Generally, the angle-resolved tangential velocities appear to be either under- or over-predicted in the trailing vortex core using the RANS models but the agreement is fairly good. The deviations might be attributed to the strongly anisotropic flow within the trailing vortices, thus demanding the application of a more elaborate turbulence model like DES or LES. The DES model has great potential to predict accurately the tangential velocity just before the vortex core, as shown in Figures 6A (at 19°), B (at 40° and 49°). This is due to the fact that the large eddies are resolve directly by DES away from boundary layer. Predictions of the k-ε model for the angle-resolved tangential velocity are also in reasonable agreement to Derksen et al.'s[29] measurements with $\sim$ 10% deviation. The V_θ are predicted well within the centre region of the vortex core when the DES and k-ε models are used but predictions by LES is not very good. Finding from this work suggest that k-ε model performed better than unresolved LES.

Predictions of angle-resolved radial velocity are also affected by the vortex core in a fashion similar to the angle-resolved tangential velocity as shown in Figures 7A, B. Of the turbulence models tested, DES was found to have the upper hand in predicting the angle-resolved radial velocity with error consistently around 10%. However, predictions of the k-ε were also in close agreement ($\sim$ 10% error) with the experimental data. Predictions by LES is not outstanding with deviation up to 50%, especially within the vortex core close to the impeller tip as shown in Figure 7A (at 31° and 40°).

Figures 8A, B show the prediction of angle-resolved axial velocities. Predictions of k-ε model is in reasonably good agreement with the experimental data ($\sim$ 10% error), although on occasion, there is a minor discrepancy in their predictions near the impeller centerline ($z = 0$; see Figure 8A at 31°). Prediction from the LES is not as good as the DES and k-ε because the flow around the boundary layer is not resolved properly, which affects the flow field development around the impeller discharge region. The DES prediction of the angle-resolved axial velocity is also not uniformly good, e.g., see Figure 8A at 40°, but overall the DES model

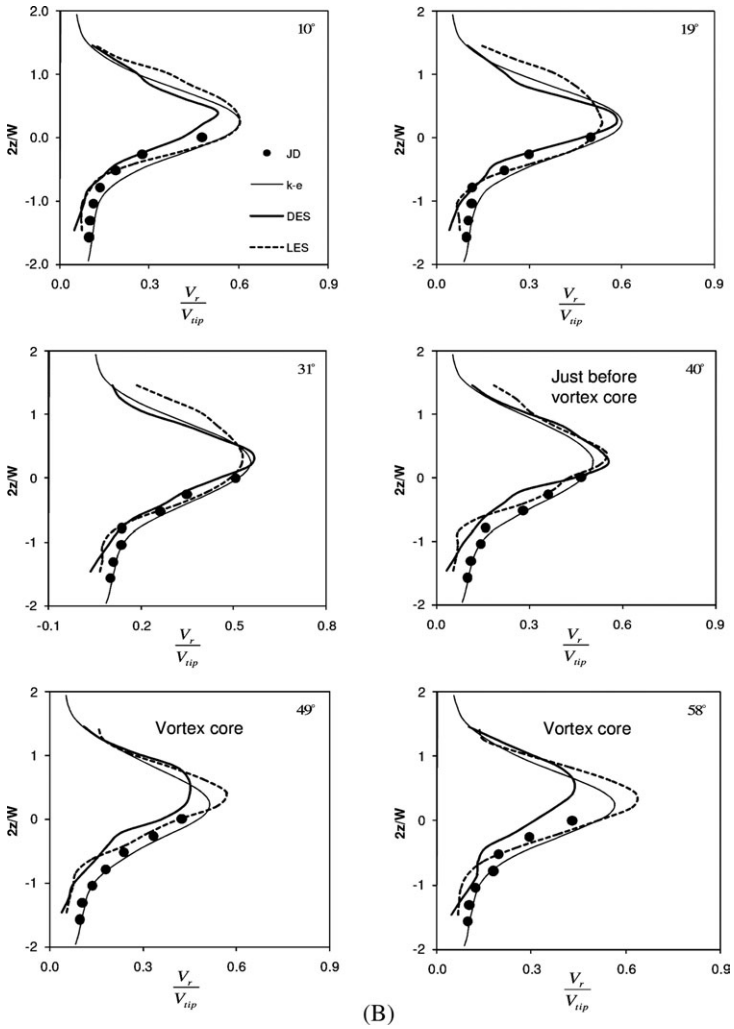

(B)

Figure 7. (Continued)

is the most consistent model for predicting the angle-resolved axial velocity.

The periodic components are the fluctuations due to blade passage meanwhile the resolved fluctuating components are the random turbulence excluding the effect of the impeller blade. The angle-resolved values of the random turbulent kinetic energy can be obtained from:

$$k_{\mathrm{ran}}(\theta) = \frac{1}{2}\left(\left\langle u_i^2\right\rangle_\theta - \left\langle u_i\right\rangle_\theta^2\right) \tag{18}$$

where $\langle\rangle_\theta$ denotes the average value at angular position θ. It is well-known that predictions of the k-ε model, and its variants, for the turbulent kinetic energy at positions farther away from impeller are in better agreement with experimental measurements, as the turbulence becomes more isotropic away from the impeller. However, they are consistently reported to under-predict the turbulent kinetic energy close to the impeller, especially in the discharge region. CFD predictions of $k_{\mathrm{ran}}(\theta)$ are shown in Figures 9A, B. Predictions of $k_{\mathrm{ran}}(\theta)$ by the k-ε model in this study are also consistent with the previous findings in ''Time-averaged predictions'' section; the predicted $k_{\mathrm{ran}}(\theta)$ values at $2r/D = 1.52$ are closer to Derksen et al.'s data ($\sim$ 20% error) than those at $2r/D = 1.3$ ($\sim$ 30% error). In contrast to the angle-resolved tangential velocity, the prediction of $k_{\mathrm{ran}}(\theta)$ is not affected by the position of the vortex core. The position relative to the impeller seems to be a more important factor for $k_{\mathrm{ran}}(\theta)$ predictions in stirred tanks, showing that the wakes behind the blades induce a highly anisotropic flow and at points far away from impeller the flow tends to be more isotropic. DES has success in predicting $k_{\mathrm{ran}}(\theta)$, as it is consistently shown to be superior compared with k-ε model in this study (see Figure 9). The LES model manages to predict the $k_{\mathrm{ran}}(\theta)$ better than the k-ε model, despite the problem of boundary layer resolution. The effect of the unresolved boundary layers on the LES prediction is only prominent close to the impeller blades.

Spectral analysis

A power spectral analysis of the instantaneous tangential velocity was carried out to investigate if an inertial subrange could be identified and if the turbulence was resolved into the inertial subrange as is required for DES and LES. The power spectrum curve was produced by doing a fast Fourier transform (FFT) on the time-series data recorded from points close to the impeller. Figure 10 depicts the power spectral density obtained at two locations in the tank, for the DES and LES of the flow generated by a Rushton turbine. The energy spectrum of the tangential

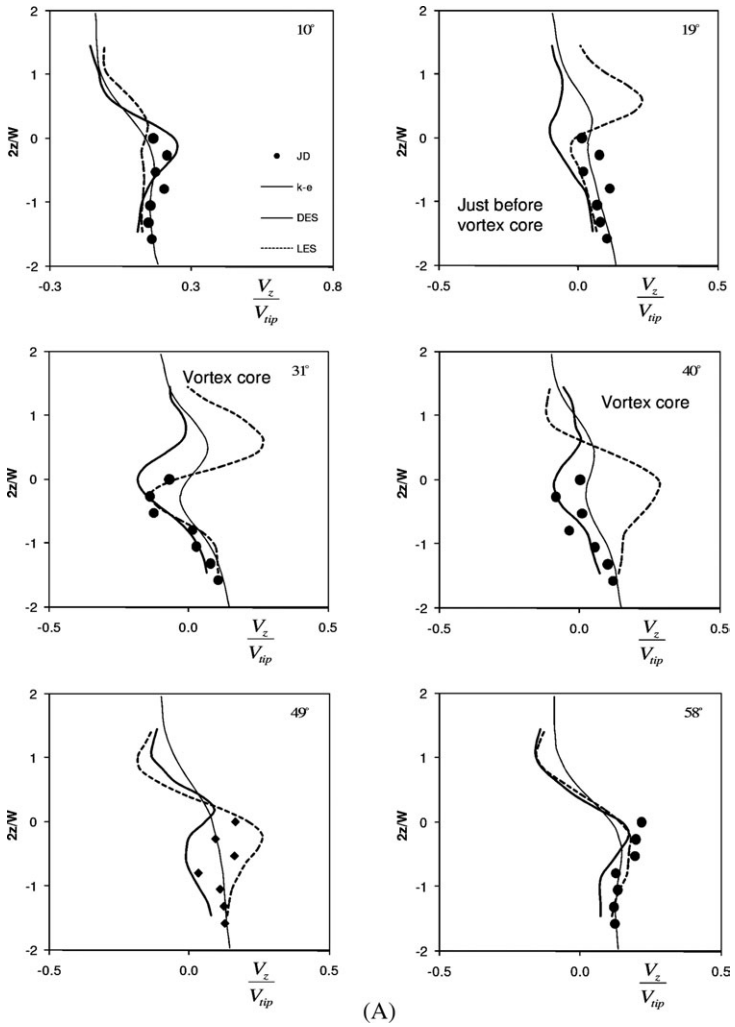

Figure 8. Prediction of the angle-resolved axial velocity for different angle positions: (A) at radial position $2r/D$ = 1.3, (B) at radial position $2r/D$ = 1.52.

JD corresponds to LDA data from Derksen et al.[29]

velocity in the impeller discharge region ($2r/D = 1.1$ and 1.52), in Figure 10, exhibits the ($-5/3$) slope typical of the inertial subrange of turbulence in the range $f/N \approx 1$–20, but then some part of the small scale turbulence ($f/N > 20$) is not fully resolved as expected. A finer grid would help to resolve more of the spectrum away from impeller, but then this is not affordable to run using a personal computer at high Reynolds number at the moment. The LES spectrum also indicates the $-5/3$ slope which confirms the reason of a reasonably good prediction of turbulent kinetics energy in this work. The sharp peaks in the spectrum at $f/N \approx 5.9$ Hz shown in Figures 10A, B are associated with the passage of the blades at every 1/6th of an impeller revolution. The FFT results indicate that the current DES and LES can resolve the turbulence in stirred tanks slightly into the inertial subrange.

Power number prediction

The power number in a stirred tank can be estimated either by integrating the dissipation rate over the tank volume, or from a calculation of the moments acting on the shaft and impeller or baffles and tank wall. The calculated torque, Γ, is then related to the power input by;

$$P = 2\pi N\Gamma \tag{19}$$

The turbulent power number was found to be dependent on impeller blade thickness by Rutherford et al.[49] For a Rushton turbine operating in a single-phase system, Rutherford et al.[49] suggested the following correlation for estimation of N_{p0}:

$$N_{p0} = 6.405 - 55.673\left(\frac{t}{D}\right) \tag{20}$$

where t is the impeller thickness and T is the tank diameter (m).

Rutherford et al.[49] carried out experimental measurements on the power number of Rushton turbines of different impeller thickness ($0.0082 < t/D < 0.034$) in a tank of $H = T =$ 0.294 m. The power number at Re = 29,000 was 4.99, obtained from interpolation of Rutherford et al.[49] data, for an impeller thickness of $t/D = 0.0204$ (very close to Derksen

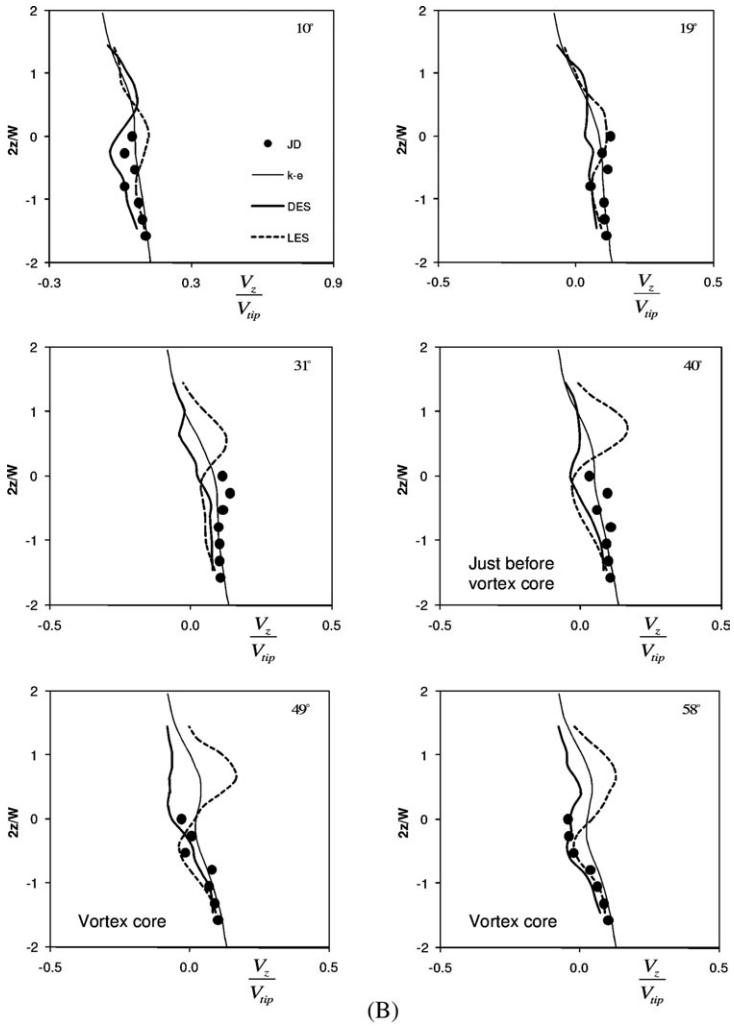

(B)

Figure 8. (Continued).

et al.'s geometry, $t/D = 0.0208$). Earlier, Yianneskis et al.[1] reported $N_{p0} = 4.96$ for an similar geometry to that used by Rutherford et al.[49] Rutherford's correlations give 5.25 for the geometry evaluated in this work—the same geometry as used by Derksen et al.[29]

The CFD predictions of the power number of a Rushton turbine are presented in Table 1. As expected, the calculation using the moment method Eq. 19 gives the better result compared with the ε integration methods, which lead to a large under-prediction (<20%) of the experimental value. The reason for the under-prediction in the ε integration method is attributed to the under-prediction of the local ε value by the RANS model; although angle-averaged ε values were predicted well by k-ε near the impeller, they may be under-predicted in the other parts of the tank. No comparison was made using the ε integration for DES and LES because the value of ε is not readily available and solving them would require a computer intensive data processing for the whole domain.

The power number estimated by the moment method gives a much closer value to published measurements,[1,49] with an average error of less than 10%. The estimated power number from either shaft and impeller or baffle and tank wall should be similar, provided that angular momentum conservation is satisfied. Such evidence can be observed for the k-ε model, where isotropic turbulence is assumed and a steady-state solver is used, but it is not quite the case for LES and DES (see Table 1) which uses the nonisotropic turbulence assumption. In this case, it might be expected that calculation of the torque from the shaft and blades might be more reliable, because of the grid refinement applied around the impeller which account for about 99% of the resultant torque.

All the RANS models gave an almost similar value of power number either by calculating the moment on the wall and baffles or impeller and shaft; overall, calculations from the impeller and shaft were in better agreement with the experiments. Nevertheless, there is not a significant difference among the predicted power numbers by any model tested in this study, suggesting that the choice of the turbulence model is not something crucial for power number estimation, at least not from torque-based methods.

Conclusions

In this study, the performance of a number of turbulence models available in the commercial CFD package Fluent (Version 6.2) was tested with respect to predicting the details of the flow in the near vicinity of Rushton turbine blades

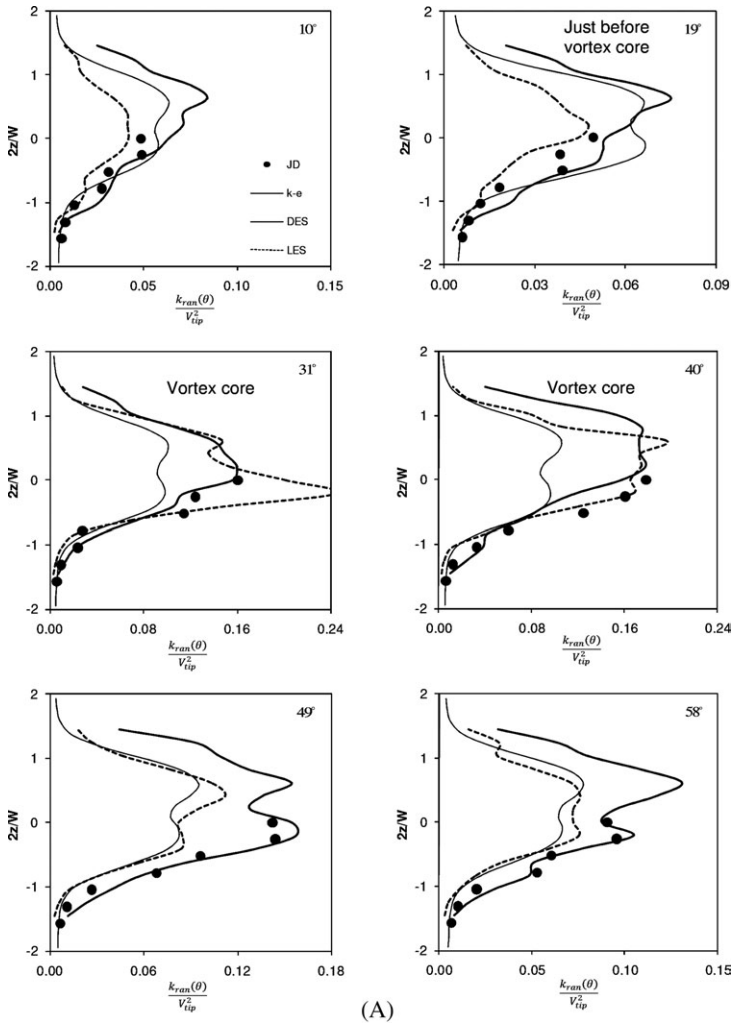

Figure 9. Prediction of the angle-resolved turbulent kinetic energy for different angle positions: (A) $k_r(\theta)$, at radial position $2r/D = 1.3$, (B) $k_r(\theta)$, at radial position $2r/D = 1.52$.

JD corresponds to LDA data from Derksen et al.[29]

with the single-phase mixing tank operating at $Re = 29{,}000$. More specifically, it was investigated to what extent predictions benefit from the improved (compared with standard LES) wall treatment of DES.

The vortex structure associated with the impeller has a great influence on the prediction of the radial and tangential velocities, as shown in this work. This feature might have been missed by previous researchers who have found that the k-ε model either under- or over-predicted the tangential velocity in a stirred tank. In fact, both the radial and tangential velocities are predicted well by the k-ε model, except in the immediate vicinity of the trailing vortex core. In the case of a Rushton turbine, where the vortex core moves radially outward, the time-averaged tangential velocity can be well predicted by the k-ε model.

Radial and axial positions of the lower and upper trailing vortex cores for a Rushton turbine have been successfully elucidated using DES. Both trailing vortices were also predicted moving in the upward axial direction, in good agreement with measurements from the literature. The accuracy of power number predictions is not strongly affected by the choice of the turbulence model. Power numbers were reasonably well predicted by any of the turbulence models used in this work, as long as the torque-method was used to calculate the power number.

Prediction of the turbulent kinetic energy very close to the impeller tip is still an issue in a stirred tank; it is under-predicted by the k-ε model. DES can predict the turbulent kinetic energy in the impeller discharge region much better than k-ε, provided a sufficiently fine grid is applied.

This study has uncovered the great potential for DES in predicting accurately the turbulent flow in a stirred tank. However, further attention to the computational grid and tentatively some improvement to the DES model might be necessary, especially regarding the turbulent viscosity model which is suspected of causing under-predictions of turbulent dissipation rates. This suggests that there is room for improvement on the current DES model in order to get a better prediction of turbulent flows especially when a standard wall function is applied. The DES is also shown to work well for a relatively coarse grid ($y^+ \sim 20$), where the LES

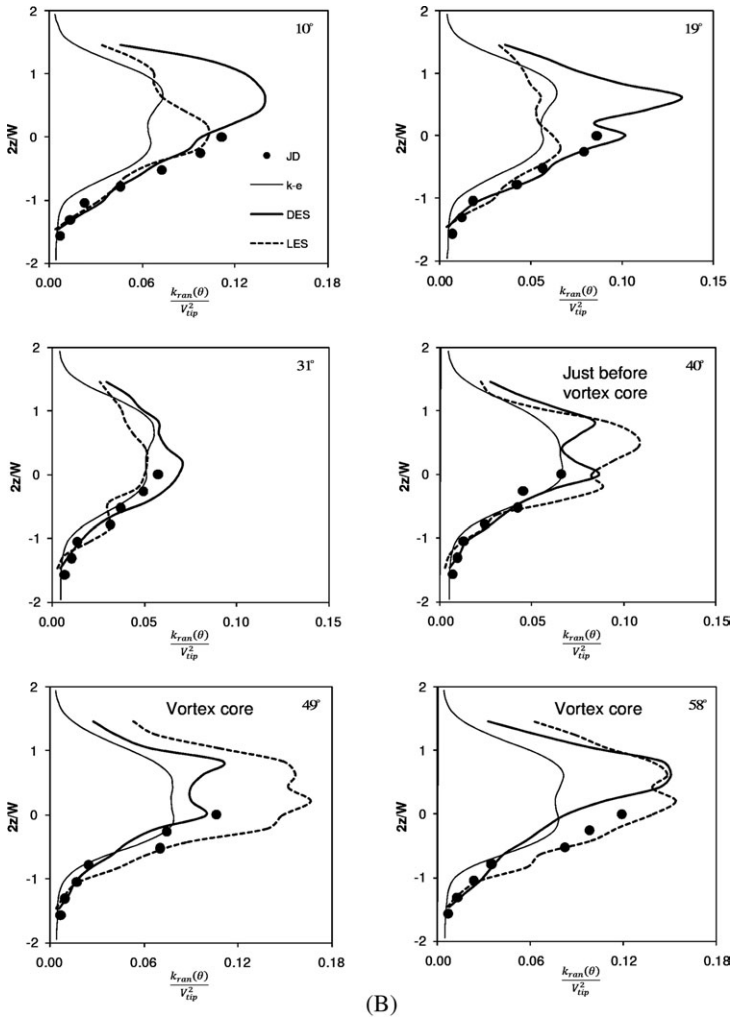

(B)

Figure 9. (Continued)

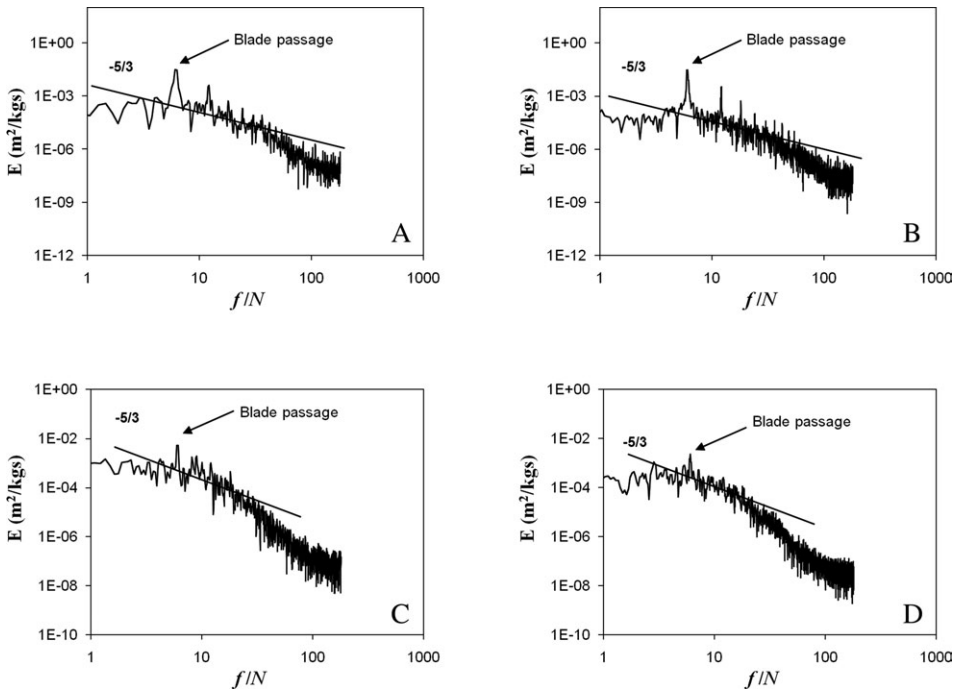

Figure 10. Power spectrum from the DES at $2z/W = -1.57$ using the instantaneous tangential velocity for $N = 3.14$ rev/s: (A) DES $2r/D = 1.1$, (B) LES $2r/D = 1.1$, (C) DES $2r/D = 1.52$, and (D) LES $2r/D = 1.52$.

Table 1. Prediction of Power Number of a Rushton Turbine

	Moment Acting on Impeller and Shaft	Moment Acting on Wall and Baffle	ε Integration
k-ε	4.72	4.73	3.99
DES	5.00	5.56	
LES	5.42	5.32	
Ref. 49*	5.25		
Ref. 49	4.99		
Ref. 1	4.87		

*Calculated from Eq. 20.

fails to perform as well. The ability of DES to tolerate a coarser grid means a significant reduction in the computational effort for turbulent flow modeling in stirred tanks compared with a fully resolved LES.

Acknowledgments

The author (J.G.) is grateful to the scholarship from Ministry of Higher Education, Malaysia, and Universiti Malaysia Pahang. The author also acknowledges contributions from Professor Harry Van den Akker and Dr. Henk Versteeg in shaping up the content of this article as his thesis examiner.

Literature Cited

1. Yianneskis M, Popiolek Z, Whitelaw JH. Experimental study of the steady and unsteady flow characteristics of stirred reactors. *J Fluid Mech*. 1987;175:537–555.
2. Ranade VV, Joshi JB. Flow generated by a disc turbine. II. Mathematical modelling and comparison with experimental data. *Chem Eng Res Des*. 1990;68:34–50.
3. Harris CK, Roekaerts D, Rosendal FJJ, Buitendijk FGJ, Daskopoulos P, Vreenegoor AJN, Wang H. Computational fluid dynamics for chemical reactor engineering. *Chem Eng Sci*. 1996;51:1569–1594.
4. Brucato A, Ciofalo M, Grisafi F, Micale G. Numerical prediction of flow fields in baffled stirred vessels: a comparison of alternative modelling approaches. *Chem Eng Sci*. 1998;53:3653–3684.
5. Patwardhan AW. Prediction of flow characteristics and energy balance for a variety of downflow impellers. *Ind Eng Chem Res*. 2001;40:3806–3816.
6. Jones RM, Harvey AD III, Acharya S. Two-equation turbulence modeling for impeller stirred tanks. *J Fluids Eng*. 2001;123:640–648.
7. Jaworski Z, Zakrzewska B. Modelling of the turbulent wall jet generated by a pitched blade turbine impeller: the effect of turbulence model. *Chem Eng Res Des*. 2002;80:846–854.
8. Aubin J, Fletcher DF, Xuereb C. Modeling turbulent flow in stirred tanks with CFD: the influence of the modeling approach, turbulence model and numerical scheme. *Exp Therm Fluid Sci*. 2004;28:431–445.
9. Li M, White G, Wilkinson D, Roberts KJ. LDA measurements and CFD modeling of a stirred vessel with a retreat curve impeller. *Ind Eng Chem Res*. 2004;43:6534–6547.
10. Ochieng A, Onyango MS, Kumar A, Kiriamiti K, Musonge P. Mixing in a tank stirred by a Rushton turbine at a low clearance. *Chem Eng Process*. 2008;47:842–851.
11. Verzicco R, Fatica M, Iaccarino G, Orlandi P. Flow in an impeller-stirred tank using an immersed-boundary method. *AIChE J*. 2004;50:1109–1118.
12. Sbrizzai F, Lavezzo V, Verzicco R, Campolo M, Soldati A. Direct numerical simulation of turbulent particle dispersion in an unbaffled stirred-tank reactor. *Chem Eng Sci*. 2006;61:2843–2851.
13. Revstedt J, Fuchs L, Tragardh C. Large eddy simulations of the turbulent flow in a stirred reactor. *Chem Eng Sci*. 1998;53:4041–4053.
14. Derksen J, Van Den Akker HEA. Large eddy simulations on the flow driven by a Rushton turbine. *AIChE J*. 1999;45:209–221.
15. Derksen J. Assessment of large eddy simulations for agitated flows. *Chem Eng Res Des*. 2001;79:824–830.
16. Yeoh SL, Papadakis G, Yianneskis M. Numerical simulation of turbulent flow characteristics in a stirred vessel using the LES and RANS approaches with the sliding/deforming mesh methodology. *Chem Eng Res Des*. 2004;82:834–848.
17. Hartmann H, Derksen JJ, Montavon C, Pearson J, Hamill IS, van den Akker HEA. Assessment of large eddy and RANS stirred tank simulations by means of LDA. *Chem Eng Sci*. 2004;59:2419–2432.
18. Li Z, Gao Z, Smith JM, Thorpe RB. Large eddy simulation of flow fields in vessels stirred by dual rushton impeller agitators. *J Chem Eng Jpn*. 2007;40:684–691.
19. Jahoda M, Mostek M, Kukukova A, Machon V. CFD modelling of liquid homogenization in stirred tanks with one and two impellers using large eddy simulation. *Chem Eng Res Des*. 2007;85:616–625.
20. Tyagi M, Roy S, Harvey AD III, Acharya S. Simulation of laminar and turbulent impeller stirred tanks using immersed boundary method and large eddy simulation technique in multi-block curvilinear geometries. *Chem Eng Sci*. 2007;62:1351–1363.
21. Yapici K, Karasozen B, Schäfer M, Uludag Y. Numerical investigation of the effect of the Rushton type turbine design factors on agitated tank flow characteristics. *Chem Eng Process*. 2007;47:1340–1349.
22. Delafosse A, Line A, Morchain J, Guiraud P. LES and URANS simulations of hydrodynamics in mixing tank: comparison to PIV experiments. *Chem Eng Res Des*. 2008;86:1322–1330.
23. Alcamo R, Micale G, Grisafi F, Brucato A, Ciofalo M. Large-eddy simulation of turbulent flow in an unbaffled stirred tank driven by a Rushton turbine. *Chem Eng Sci*. 2005;60:2303–2316.
24. Addad Y, Gaitonde U, Laurence L, Rolfo S, Optimal unstructured meshing for large eddy simulations, In: *Quality and Reliability of Large-Eddy Simulations, ERCOFTAC SERIESERCOFTAC Series,* 2008;12:93–103.
25. Squires KD, Forsythe JR, Spalart PR. Detached-eddy simulation of the separated flow over a rounded-corner square. *J Fluids Eng*. 2005;127:959–966.
26. Spalart PR, Jou W-H, Strelets M, Allmaras SR. Comments on the feasibility of LES for wings, and on a hybrid RANS/LES Approach. In: *Advances in DNS/LES, 1st AFOSR International Conference on DNS/LES*, August 4–8, Columbus, OH: Greyden Press, 1997.
27. Spalart PR. Young-Person's Guide to Detached-Eddy Simulation Grids, Technical Report. NASA/CR-2001-211032. 2001.
28. Spalart PR. Detached-eddy simulation. *Annu Rev Fluid Mech*. 2009;41:181–202.
29. Derksen JJ, Doelman MS, Van Den Akker HEA. Three-dimensional LDA measurements in the impeller region of a turbulently stirred tank. *Exp Fluids*. 1999;27:522–532.
30. Fluent Inc. *Gambit 2.2 Documentation*. Fluent Inc., 2004.
31. Launder BE, Spalding DB. Numerical computation of turbulent flows. *Comput Methods Appl Mech Eng*. 1974;3:269–289.
32. Smagorinsky J. General circulation experiments with the primitive equations. I. The basic experiment. *Mon Weather Rev*. 1963;91:99–164.
33. Lilly DK. On the application of the eddy viscosity concept in the inertial subrange of turbulence, Technical Report. NCAR Manuscript 123. 1966.
34. Spalart PR, Allmaras SR. A One-Equation Turbulence Model for Aerodynamic Flows. AIAA Paper 92-0439. 1992.
35. Luo JY, Issa RI, Gosman AD. Prediction of impeller-induced flows in mixing vessels using multiple frames of reference. *IChemE Symp Ser* 1994;136:549–556.
36. Fluent Inc. *Fluent 6.2 User Guide*. Fluent Inc. 2005.
37. Patankar SV. *Numerical Heat Transfer and Fluid Flow*. Great Britain: Taylor & Francis, 1980.
38. Gimbun J, Rielly CD, Nagy ZK. Modelling of mass transfer in gas–liquid stirred tanks agitated by Rushton turbine and CD-6 impeller: a scale-up study. *Chem Eng Res Des*. 2009;87:437–451.
39. Nere NK, Patwardhan AW, Joshi JB. Prediction of flow pattern in stirred tanks: new constitutive equation for eddy viscosity. *Ind Eng Chem Res*. 2001;40:1755–1772.
40. Luo H. Coalescence, breakup and liquid circulation in bubble column reactors, D.Sc. Thesis, Norwegian Institute of Technology, 1993.
41. Luo H, Svendsen HF. Theoretical model for drop and bubble breakup in turbulent dispersions. *AIChE J*. 1996;42:1225–1233.
42. Prince MJ, Blanch HW. Bubble coalescence and break-up in air-sparged bubble columns. *AIChE J*. 1990;36:1485–1499.

43. Ranade VV, Perrard M, Le Sauze N, Xuereb C, Bertrand J. Trailing vortices of Rushton turbine: PIV measurements and CFD simulations with snapshots approach. *Chem Eng Res Des*. 2001;79:3–12.
44. Lee KC, Yianneskis M. Turbulence properties of the impeller stream of a Rushton turbine. *AIChE J*. 1998;44:13–24.
45. Yoon HS, Balachandar S, Ha MY, Kar K. Large eddy simulation of flow in a stirred tank. *J Fluids Eng*. 2003;125:486–499.
46. Escudie' R, Bouyer D, Line' A. Characterization of trailing vortices generated by a Rushton turbine. *AIChE J*. 2004;50:75–86.
47. Jeong J, Hussain F. On the identification of a vortex. *J Fluid Mech*. 1995;285:69–94.
48. Stoots CM, Calabrese RV. Mean velocity field relative to a Rushton turbine blade. *AIChE J*. 1995;41:1–11.
49. Rutherford K, Mahmoudi SMS, Lee KC, Yianneskis M. The influence of Rushton impeller blade and disk thickness on the mixing characteristics of stirred vessels. *Chem Eng Res Des*. 1996;74:369–378.

Manuscript received May 28, 2011, and revision received Oct. 8, 2011.